

# COULD A MULTI-PEV NEUTRINO EVENT HAVE AS ORIGIN THE INTERNAL SHOCKS INSIDE THE GRB PROGENITOR STAR?

N. FRAIJA<sup>1</sup>

Instituto de Astronomía, UNAM, México, 04510

*Draft version March 3, 2024*

## ABSTRACT

The IceCube Collaboration initially reported the detection of 37 extraterrestrial neutrinos in the TeV - PeV energy range. The reconstructed neutrino events were obtained during three consecutive years of data taking, from 2010 to 2013. Although these events have been discussed to have an extragalactic origin, they have not been correlated to any known source. Recently, the IceCube Collaboration reported a neutrino-induced muon event with energy of  $2.6 \pm 0.3$  PeV which corresponds to the highest event ever detected. Neither the reconstructed direction of this event (J2000.0), detected on June 11 2014 at R.A.=110°.34, Dec.=11°.48 matches with any familiar source. Long gamma-ray bursts (IGRBs) are usually associated with the core collapse of massive stars leading relativistic-collimated jets inside stars with high-energy neutrino production. These neutrinos have been linked to the 37 events previously detected by IceCube experiment. In this work, we explore the conditions and values of parameters so that the highest neutrino recently detected could be generated by proton-photon and proton-hadron interactions at internal shocks inside IGRB progenitor star and then detected in IceCube experiment. Considering that internal shocks take place in a relativistic collimated jet, whose (half) opening angle is  $\theta_0 \sim 0.1$ , we found that IGRBs with total luminosity  $L \lesssim 10^{48}$  erg/s and internal shocks on the surface of progenitors such as Wolf-Rayet (WR) and blue super giant (BSG) stars favor this multi-PeV neutrino production, although this neutrino could be associated to  $L \sim 10^{50.5}$  ( $\sim 10^{50}$ ) erg/s provided that the internal shocks occur at  $\sim 10^9$  ( $\sim 10^{10.2}$ ) cm for a WR (BSG).

*Subject headings:* Gamma-ray burst: general - stars: interiors - stars: jets - neutrinos

## 1. INTRODUCTION

The IceCube Collaboration has reported evidence for extragalactic neutrinos. They announced, firstly, two shower-like events of PeV neutrinos (Aartsen et al. 2013), after 24 events (19 shower-like, and the remainder track-like; IceCube Collaboration (2013)) and finally 11 events were added to these detections (Aartsen et al. 2014). In the aggregate, 37 events (9 track-like and 28 shower-like) were detected after analyzing three year data (2010 to 2013; Aartsen et al. (2014)). The excess measured over the atmospheric background had a statistical significance  $5.7\sigma$ . Arrival directions of these neutrino events seem to be isotropic and nonneutrino track-like has been associated with the location of known sources yet. Recently, a multi-PeV neutrino-induced muon event detected in 2014 June 11 was reported by the IceCube Collaboration (Schoenen & Raedel 2015). The neutrino with an energy  $2.6 \pm 0.3$  PeV is the highest-energy event ever detected. This event had a probability of less than 0.01% of having an atmospheric origin, hence putting together in a sky map this event with the known sources as shown in Figure 1, the reconstructed direction of this event (J2000.0: R.A.=110°.34, Dec.=11°.48) does not match with any of the known sources.

Long gamma-ray bursts (IGRBs) have been generally linked to core collapse of massive stars leading to relativistic-collimated jets and supernovae (CCSNe) of type Ib,c and II. Type II and Ib are widely believed to have a radius of  $R_* \approx 3 \times 10^{12}$  cm, usually associated with blue super giant (BSG) stars, and type Ic supernovae are thought to be Wolf-Rayet (WR) stars with radius  $R_* \approx 10^{11}$  cm. Depending on the luminosities and durations, successful IGRBs have revealed a variety of GRB populations: low-luminosity (ll), ultra-long (ul) and high-luminosity (hl) GRBs (Mészáros & Waxman 2001; Liang et al. 2007; Gendre et al. 2013). While llGRBs and ulGRBs have a typical duration of ( $\sim 10^3$  s), hlGRBs have a duration of tens to hundreds of seconds. Another relevant population associated with CCSNe, although unobservables in photons, are failed GRBs which could be much more frequent than successful ones, limited only by the ratio of type Ib/c and type II SNe to GRBs rates. This population has been identified by having high-luminosities, mildly relativistic jets and durations from some to ten seconds (Huang et al. 2002; Mészáros & Waxman 2001; Soderberg & et al. 2006, 2010).

Many astrophysical environments have been explored to explain these high-energy (HE) neutrinos. For instance, GRB (Murase & Ioka 2013; Razzaque 2013; Fraija 2014; Liu & Wang 2013; Tamborra & Ando 2015a; Petropoulou et al. 2014; Tamborra & Ando 2015b), active galactic nuclei (AGN; Dermer et al. (2014); Stecker (2013); Petropoulou et al. (2015); Padovani et al. (2015)), dark matter (DM; Feldstein et al. (2013); Esmaili & Dario Serpico (2013)) and cosmic neutrino background connections (Ioka & Murase 2014; Ng & Beacom 2014).

GRBs have been widely pointed out as emitter sources of HE neutrinos in connection to cosmic rays accelerated up to ultra high energies (Milgrom & Usov 1995; Waxman 1995b,a; Waxman & Bahcall 1999; Waxman 2000b,a; Vietri 1997; Rachen & Mészáros 1998; Böttcher & Dermer 1998).

Recently, Murase & Ioka (2013) studied HE neutrino production in collimated jets inside progenitors of IGRBs, considering both collimation and internal shocks. Authors showed that whereas classical GRBs may be too powerful to generate HE neutrinos

nifraija@astro.unam.mx

<sup>1</sup> Instituto de Astronomía, Universidad Nacional Autónoma de México, Circuito Exterior, C.U., A. Postal 70-264, 04510 México D.F., México

inside stars, low-power (lp) GRBs (including llGRBs) were candidates for producing the HE neutrinos reported by the IceCube collaboration.

One major progress in recent years has been the realization that photon emission from the photosphere, namely optically thick regions may be relevant to GRBs. Clearly, the photosphere marks the point below which the plasma is optically thick and above which it is optically thin. Several theoretical works in recent years dealt with the properties of shock waves that propagate in optically thick regions - the so called "radiation mediated shocks" (Budnik et al. 2010; Katz et al. 2010; Bromberg et al. 2011a; Levinson 2012). These authors have argued, that the properties of these radiation mediated shocks in the depth of the star are such that do not allow them to accelerate protons up to HEs.

In this work, we explore the conditions under which the highest neutrino recently detected at 2.6 PeV could be created by hadronic interactions in internal shocks inside a GRB progenitor star. In section II, we show the dynamics of jet, internal shocks, particle acceleration process and the neutrino production by proton-photon (p- $\gamma$ ) and proton-hadron (p-h) interactions. In section III, we explain the neutrino flux expected on IceCube detector from p- $\gamma$  and p-h interactions. In section IV we discuss our results and in section V we give a brief conclusions. We hereafter use primes (unprimes) to define the quantities in a comoving (observer) frame,  $Q_x \equiv Q/10^x$  in c.g.s. units and  $k = \hbar=c=1$  in natural units.

## 2. INTERNAL SHOCKS AND NEUTRINO PRODUCTION

In GRB context, one of the most prosperous theory to explain the prompt emission and the afterglow is the fireball model (Zhang & Mészáros 2004; Mészáros 2006). In this model, the prompt emission is explained through internal shell collisions, where faster shells ( $\Gamma_f$ ) catch slower shells ( $\Gamma_s$ ). These internal shocks take place at a distance of  $r_j = 2\Gamma^2 t_\nu$ , with  $t_\nu$  given by the variability time scale of the central object and  $\Gamma \simeq \sqrt{\Gamma_f \Gamma_s}$  the bulk Lorentz factor of the propagating shock. We are interested in those internal shocks that occur inside the star ( $r_j < R_*$  with  $R_*$  the radius of the progenitor's stellar surface) and the hydrodynamic jet is collimated by the cocoon pressure via collimation shocks (Bromberg et al. 2011b; Mizuta & Ioka 2013). It happens when the jet luminosity is low and/or density is high for an initial opening angle. The total energy density  $U = 1/(8\pi m_p) \Gamma^{-4} L t_\nu^{-2}$  in internal shocks is equipartitioned to amplify the magnetic field

$$B' = \epsilon_B^{1/2} \Gamma^{-2} L^{1/2} t_\nu^{-1}, \quad (1)$$

with  $\epsilon_B = U_B/U = (B^2/8\pi)U$  and accelerate particles  $\epsilon_i = U_i/U$ , where  $i$  is the  $i$ th kind of particle with the condition  $\epsilon_B + \sum_i \epsilon_i = 1$ . Electrons are accelerated in internal shocks and then are cooled down rapidly by synchrotron radiation in the presence of the magnetic field. The synchrotron photons in this length scale produce an opacity to Thomson scattering given by  $\tau'_{th} = \frac{\sigma_T}{4\pi m_p} \Gamma^{-3} L t_\nu^{-1}$  where  $\sigma_T$  is the Thompson cross section and  $m_p$  is the proton mass. Photons can thermalize in a black body temperature with peak energy given by

$$T'_\gamma \simeq \frac{1.2}{\pi} \epsilon_e^{1/4} L^{1/4} \Gamma^{-1} t_\nu^{-1/2}. \quad (2)$$

The proton distribution is cooled down in internal shocks via electromagnetic (synchrotron radiation and inverse Compton (IC) scattering) and hadronic p- $\gamma$  and p-h interactions channels. P- $\gamma$  and p-h interactions take place when accelerated protons interact with thermal keV photons and proton density at the shock. In both interactions HE charged pions and kaons are produced;  $p + \gamma/h \rightarrow X + \pi^\pm/K^\pm$ , and subsequently HE neutrinos  $\pi^+ \rightarrow \mu^+ + \nu_\mu \rightarrow e^+ + \nu_e + \bar{\nu}_\mu + \nu_\mu$  and  $\pi^- \rightarrow \mu^- + \bar{\nu}_\mu \rightarrow e^- + \bar{\nu}_e + \nu_\mu + \bar{\nu}_\mu$ .

### 2.1. Particle acceleration process

Before the jet breaks out the star, it keeps the bulk Lorentz factor low by converging cylindrically via collimation shocks under the cocoon pressure. The characteristic radius to which the shocked jet becomes cylindrical is (Bromberg et al. 2011b)

$$r_c = \left[ \frac{3\epsilon_c^2}{16\pi^{3/2}\eta_c\chi_c} \right]^{1/5} t^{2/5} L_j^{3/10} \theta_0^{4/5} \rho_a^{-3/10}, \quad (3)$$

where  $\rho_a$  is the ambient density,  $\theta_0$  is initial opening angle,  $\epsilon_c = \frac{5}{3+\alpha_\delta}$ ,  $\eta_c = \frac{3}{3-\alpha_\delta}$  and  $\chi_c = \frac{5}{7-\alpha_\delta}$ . Here,  $L_j = \theta_0^2 \frac{L}{4}$  is the absolute jet luminosity defined through the total luminosity  $L$ . In the meantime, the position of the non-relativistic head is

$$r_h = \left[ \frac{16\eta_h\zeta_h^2}{3\pi} \right]^{1/5} t^{3/5} L_j^{1/5} \theta_0^{-4/5} \rho_a^{-1/5}, \quad (4)$$

where  $\eta_h = \frac{3}{3-\alpha_\delta}$  and  $\zeta_h = \frac{5-\alpha_\delta}{3}$ . We consider density profiles as

$$\rho_a \simeq \begin{cases} \frac{(3-\alpha)M_*}{4\pi R_*^3} \left( \frac{r}{R_*} \right)^{-\alpha_\delta} & \text{for WR} \\ \rho_0 K & \text{for BSG,} \end{cases} \quad (5)$$

with  $K$  given by  $\left( \frac{R_*}{r} \right)^{17/7}$  for  $r_a < r < r_b$  and  $\left( \frac{R_*}{r} \right)^{17/7} \left( \frac{r-R_*}{r_b-R_*} \right)^5$  for  $r > r_b$ . Here  $\rho_0 = 3.4 \times 10^{-5} \text{ g cm}^{-3}$ ,  $r_a = 10^{10.8} \text{ cm}$ ,  $r_b = 10^{12} \text{ cm}$ ,  $M_*$  is the progenitor mass and  $\alpha_\delta = 3/2 - 3$ , being  $3/2$  and  $3$  for convective and radiative envelopes, respectively.

From eqs. (3), (4) and (5), the cylindrical and head radii for a WR are

$$\begin{aligned} r_c &= \left[ \frac{3\epsilon_c^2}{16(3-\alpha_\delta)^{3/2}\eta_c\chi_c} \right]^{\frac{2}{10-3\alpha_\delta}} t^{\frac{4}{10-3\alpha_\delta}} L^{\frac{3}{10-3\alpha_\delta}} \theta_0^{\frac{14}{10-3\alpha_\delta}} M_\star^{\frac{3}{3\alpha_\delta-10}} R_\star^{\frac{9-3\alpha_\delta}{10-3\alpha_\delta}} \\ r_h &= \left[ \frac{16\eta_h\zeta_h^2}{3(3-\alpha_\delta)} \right]^{\frac{1}{5-\alpha_\delta}} t^{\frac{3}{5-\alpha_\delta}} L^{\frac{1}{5-\alpha_\delta}} \theta_0^{\frac{2}{5-\alpha_\delta}} M_\star^{\frac{1}{\alpha_\delta-5}} R_\star^{\frac{3-\alpha_\delta}{5-\alpha_\delta}}, \end{aligned} \quad (6)$$

and for a BSG are

$$\begin{aligned} r_c &= \left[ \frac{3\epsilon_c^2}{27\pi^{3/2}\eta_c\chi_c} \right]^{1/5} t^{2/5} L^{3/10} \theta_0^{7/5} \rho_0^{-3/10} K^{-3/10} \\ r_h &= \left[ \frac{2^3\eta_h\zeta_h^2}{3\pi} \right]^{1/5} t^{3/5} L^{1/5} \theta_0^{-2/5} \rho_0^{-1/5} K^{-1/5}. \end{aligned} \quad (7)$$

Propagating shocks in optically thick regions are radiation mediated. The properties of these radiation mediated shocks in the depth of the star are such that do not allow to accelerate protons up to HEs. Upstream proton flow is decelerated by photons created in the downstream and diffusing into the upstream region (Budnik et al. 2010; Katz et al. 2010; Bromberg et al. 2011a; Levinson 2012). It happens when the deceleration scale  $l_{dec} \simeq (n_p \sigma_T y_\pm)^{-1}$  of the shock width is smaller than the comoving size ( $l_\nu$ ) of the upstream flow, as indicated by Murase & Ioka (2013). Protons, then, are expected when shock propagates in an optically thin region (radiation unmediated shock;  $l_\mu \ll l_{dec}$ ). Hence, accelerated protons are expected around the photosphere  $\tau \sim (1-10)$  (Murase 2008), as assumed in the dissipative photosphere scenario (Rees & Mészáros 2005; Murase et al. 2006). Following Murase & Ioka (2013), a reasonably necessary condition for proton acceleration is

$$\tau = n_p \sigma_T r \lesssim \min[\Gamma_{rel}^2, 0.1 C^{-1} \Gamma_{rel}^3], \quad (8)$$

where  $C = 1 + 2 \ln \Gamma_{rel}^2$ ,  $\Gamma_{rel} \approx (\Gamma_f/\Gamma + \Gamma/\Gamma_f)/2$  is the relative Lorentz factor between the faster and merged shells and  $n_p$  is the number proton density.

In this case, neutrino energy is limited by the maximum energy at accelerated protons which is obtained equaling the time scales of acceleration  $t'_{acc} = \frac{2\pi\xi B'_{c,p}}{m_p^2} E_p' \epsilon_B^{-1/2} L^{-1/2} \Gamma^2 t_v$  and cooling synchrotron  $t'_{p,syn} = \frac{6\pi m_p^4}{\sigma_T m_e^2 E_p'} \epsilon_B^{-1} L^{-1} \Gamma^4 t_v^2$ , supposing that the synchrotron process is the longest timescale (e.g. see Fraija (2014)). Hence, it can be written as

$$E_{p,max} = \left( \frac{3e m_p^4}{\sigma_T \xi m_e^2} \right)^{1/2} \epsilon_B^{-1/4} L^{-1/4} \Gamma^2 t_v^{1/2}, \quad (9)$$

where  $e$  is the electric charge,  $m_e$  is the electron mass,  $\xi$  is a factor of equality and  $B'_{c,p}$  is the critical magnetic field for protons.

### 2.2. $P$ - $\gamma$ interactions

The number density of thermalized photons  $\eta'_\gamma \simeq \frac{2\zeta(3)}{\pi^2} T'_\gamma$  can be explicitly written as

$$n'_\gamma = \frac{3.2\zeta(3)}{\pi^5} \epsilon_e^{3/4} L^{3/4} \Gamma^{-3} t_v^{-3/2}. \quad (10)$$

The optical depth characteristic for this process is  $\tau'_{p\gamma} = \frac{6.5\zeta(3)\sigma_{p\gamma}}{\pi^5} \epsilon_e^{3/4} L^{3/4} \Gamma^{-2} t_v^{-1/2}$ , where  $\zeta(x)$  is the zeta function and  $\sigma_{p\gamma}$  is the cross section of  $p$ - $\gamma$  interactions. From the resonance  $p + \gamma \rightarrow \Delta^+$  in the rest frame and taking into account that each neutrino carries 5% of the proton energies ( $E_\nu = 1/20 E_p$ ), then the threshold neutrino energy can be written as

$$E_{\nu,\pi} \simeq 10^{-1.67} \pi (m_\Delta^2 - m_p^2) \epsilon_e^{-1/4} L^{-1/4} \Gamma^2 t_v^{1/2}, \quad (11)$$

where  $m_\Delta$  is the resonance mass.

### 2.3. $P$ - $h$ interactions

Protons co-accelerated in the internal shocks have a comoving number density (Razzaque & Smirnov 2010; Razzaque et al. 2005; Ando & Beacom 2005; MacLachlan et al. 2013)

$$n'_p = 1/(8\pi m_p) \Gamma^{-4} L t_v^{-2}, \quad (12)$$

with energy density  $n'_p m_p$ . The optical depth for  $p$ - $h$  interactions is  $\tau'_{pp} \simeq \frac{\sigma_{pp}}{4\pi m_p} L \Gamma^{-3} t_v^{-1}$  where  $\sigma_{pp} = 34.3 + 1.88 S + 0.25 S^2$  mb is the cross section for these interactions with  $S = \log(E_p/TeV)$  (Kelner et al. 2006). Pions ( $\pi^\pm$ ) and kaons ( $K^\pm$ ) can be produced as products of  $p$ - $h$  interactions ( $p + h \rightarrow X + \pi^\pm/K^\pm$ ). Considering the meson lifetime and  $p$ - $h$  interaction time scale

$$t'_{had} \simeq \frac{10\pi m_p}{\sigma_{pp}} L^{-1} \Gamma^4 t_v^2, \quad (13)$$

mesons, then, in the presence of the magnetic field radiate via synchrotron radiation and also could interact with the primary protons before they decay.

### 2.3.1. Pion component

Equating the cooling synchrotron radiation  $t'_{\pi^+,syn} = \frac{6\pi m_{\pi^+}^4}{\sigma_T m_e^2} \epsilon_B^{-1} L^{-1} \Gamma^2 t_v^2 E_{\pi^+}'^{-1}$  and the lifetime of pions  $t'_{\pi^+,dec} = \frac{E_{\pi^+}'}{m_{\pi^+}} \tau_{\pi^+}$  with the hadronic time scale (eq. 13), we get neutrino break energies due to the synchrotron radiation and the lifetime of pions

$$E_{\nu,\pi^+,syn} = 1.2 \frac{m_{\pi^+}^4 \sigma_{pp}}{m_p \sigma_T m_e^2} \epsilon_B^{-1} \Gamma, \quad (14)$$

and

$$E_{\nu,\pi^+,lt} = 2.5 \frac{\pi m_p m_{\pi^+}}{\sigma_{pp}} \tau_{\pi^+}^{-1} L^{-1} \Gamma^5 t_v^2, \quad (15)$$

respectively. Here  $m_{\pi^+}$  is the charged pion mass and  $\tau_{\pi^+}$  is the lifetime of the charged pion.

### 2.3.2. Kaon component

Comparing for kaons, the cooling synchrotron radiation  $t'_{k^+,syn} = \frac{6\pi m_{k^+}^4}{\sigma_T m_e^2} \epsilon_B^{-1} L^{-1} \Gamma^2 t_v^2 E_{k^+}'^{-1}$  and the lifetime  $t'_{k^+,dec} = \frac{E_{k^+}'}{m_{k^+}} \tau_{k^+}$  with the hadronic time scale (eq. 13), we obtain neutrino break energies due to the synchrotron radiation and the lifetime of kaons

$$E_{\nu,k^+,syn} = 0.3 \times \frac{m_{k^+}^4 \sigma_{pp}}{m_p \sigma_T m_e^2} \epsilon_B^{-1} \Gamma, \quad (16)$$

and

$$E_{\nu,k^+,lt} = 2.5 \frac{\pi m_p m_{k^+}}{\sigma_{pp}} \tau_{k^+}^{-1} L^{-1} \Gamma^5 t_v^2, \quad (17)$$

respectively. Here  $m_{k^+}$  is the charged pion mass and  $\tau_{k^+}$  is the lifetime of the charged kaon.

## 3. NEUTRINO EXPECTATION

The expected number of reconstructed neutrino events in the IceCube experiment can be computed as

$$N_{ev} = T N_A \int_{E_{th}} \sigma_{\nu N} M_{eff} \frac{dN_\nu}{dE_\nu} dE_\nu, \quad (18)$$

where  $T \simeq 4$  years is the observation time,  $N_A = 6.022 \times 10^{23} \text{ g}^{-1}$  is the Avogadro number,  $\sigma_{\nu N} = 6.78 \times 10^{-35} \text{ cm}^2 (E_\nu / \text{TeV})^{0.363}$  is the neutrino-nucleon cross section (Gandhi et al. 1998) and  $M_{eff}$  is the effective target mass of the IceCube experiment (IceCube Collaboration 2013). The neutrino spectrum  $dN_\nu/dE_\nu$  is computed from p- $\gamma$  and p-h interactions as follows.

### 3.1. P- $\gamma$ interactions

The spectrum of muon neutrino generated by p- $\gamma$  interactions is (Kelner & Aharonian 2008)

$$\left( \frac{dN_\nu}{dE_\nu} \right)_{p\gamma} = \frac{V}{4\pi d_z^2} \int_{E_p} \int_{\epsilon} \frac{dN_p}{dE_p} \frac{dN_\epsilon}{d\epsilon} F_{\nu_\mu}^{p\gamma}(\eta, x) \frac{dE_p}{E_p} d\epsilon, \quad (19)$$

where  $V = \frac{4}{3}\pi r_j^3$ ,  $d_z$  is the luminosity distance from the source and the proton distribution is given by a power law

$$\frac{dN_p}{dE_p} \simeq A_p E_p^{-\alpha}, \quad (20)$$

with  $A_p \simeq n_p/\text{GeV}$ . The distribution of target photons  $dN_\epsilon/d\epsilon$  corresponds to the blackbody radiation with temperature and photon density given by eqs. (2) and (10), respectively, and the function  $F_{\nu_\mu}^{p\gamma}(\eta, x)$  is given in appendix A.

### 3.2. P-h interactions

The spectrum of muon neutrino generated by p-h interactions is (Kelner et al. 2006)

$$\left( \frac{dN_\nu}{dE_\nu} \right)_{ph} = \frac{V n_p}{4\pi d_z^2} \int_{E_p}^\infty \sigma_{pp} \frac{dN_p}{dE_p} F_{\nu_\mu}^{pp}(E_p, x) \frac{dE_p}{E_p}, \quad (21)$$

where the proton distribution  $dN_p/dE_p$  is given in eq. (20). The function  $F_{\nu_\mu} = F_{\nu_\mu}^{(1)} + F_{\nu_\mu}^{(2)}$  comes from the contribution of decay of muon  $F_{\nu_\mu}^{(1)}$  and from the direct decays of pion  $F_{\nu_\mu}^{(2)}$ . Functions  $F_{\nu_\mu}^{(1)}$  and  $F_{\nu_\mu}^{(2)}$  are explicitly written and explained in appendix B.

## 4. RESULTS

In the CCSNe-GRB connection framework, we have considered WR and bigger progenitors like BSG stars with formation of jets leading to internal shocks inside of them. In these shocks, energy is equipartitioned between magnetic fields and acceleration of particles. Electrons and protons are expected to be accelerated in these shocks and after, to be cooled down by synchrotron radiation, inverse Compton and hadronic processes (p- $\gamma$  and p-h interactions). Both thermalized photons produced by electron synchrotron radiation and hadrons at the shocks serve as targets in the neutrino production through hadronic interactions. In this model, we have shown the production channels of HE neutrinos as a function of bulk Lorentz factor, variability time scale, total luminosity and microphysical parameters ( $\epsilon_B$  and  $\epsilon_e$ ). A detailed description such as time scales for all processes (electromagnetic and hadronic) is given in [Fraija \(2014\)](#). Additionally, we have computed the number of events expected in the IceCube experiment. In Figure 2 is shown the regions for which internal shocks occur inside a WR (red region) and BSG (blue region) star. By considering the typical values of variability  $10^{-3} \leq t_\nu \leq 1$  s, we have found that the bulk Lorentz factor lies in the range  $1 \leq \Gamma \leq 40$  for a WR and  $1 \leq \Gamma \leq 220$  for a BSG. From eqs. (6) and (7), and using the typical values of  $\theta_0$  and  $L$  ([Mizuta & Ioka 2013](#)), the cylindrical and head radii for a WR and BSG can be written as

$$r_c \simeq \begin{cases} 1.01 \times 10^8 \text{ cm } t_1^{1.08} L_{51}^{0.81} \theta_{0,-1}^{3.78} M_{\star,20 M_\odot}^{-0.81} R_{\star,11}^{0.73} & \text{for WR} \\ 3.38 \times 10^9 \text{ cm } t_3^{2/5} L_{49.8}^{3/10} \theta_{0,-1}^{7/5} & \text{for BSG,} \end{cases} \quad (22)$$

and

$$r_h \simeq \begin{cases} 9.67 \times 10^{10} \text{ cm } t_1^{1.03} L_{51}^{0.35} \theta_{0,-1}^{-0.69} M_{\star,20 M_\odot}^{-0.35} R_{\star,11}^{0.31} & \text{for WR} \\ 2.29 \times 10^{12} \text{ cm } t_3^{2/5} L_{49.8}^{3/10} \theta_{0,-1}^{7/5} & \text{for BSG.} \end{cases} \quad (23)$$

Here we have used  $\alpha_\delta = 2.1$ . Taking into account the condition  $r_c < r_j$  and eq. (8), we plot contour lines of total luminosity and internal shock radius as a function of bulk Lorentz factor for which the necessary condition for proton acceleration is established in a WR (left panel) and BSG (right panel), as shown in Figure 3. From the left panel (WR), one can see that the total luminosity lies in the range  $10^{46.5} \leq L \leq 10^{50.5}$  erg/s for an internal shock radius in the range  $10^8 \leq r_j \leq 10^{11}$  cm and from the right panel (BSG), the total luminosity lies in range  $10^{46} \leq L \leq 10^{49.8}$  erg/s for a radius  $10^{10} \leq r_j \leq 10^{12.3}$  cm. When we consider the maximum values of bulk Lorentz factors  $\Gamma \sim 40$  and  $\Gamma \sim 220$  for a WR and SGB (see fig. 2), respectively, from eqs. (8) and (12), the optical depths become

$$\tau \simeq \begin{cases} 2.11 L_{(50.5-48)} r_{j,(8.3-10.8)} \Gamma_{1.53}^{-1} & \text{for WR} \\ 2.95 L_{(49.8-48)} r_{j,(10.2-12.2)} \Gamma_{2.35}^{-1} & \text{for BSG} \end{cases} \lesssim \min[\Gamma_{rel,1}^2, C^{-1} \Gamma_{rel,1}^3]. \quad (24)$$

Comparing eqs. (22) and (24), it is trivial to demonstrate that accelerated protons could be expected when  $r_c < r_j$  and total luminosity in the range  $10^{48} < L < 10^{50.5}$  erg/s ( $10^{48} < L < 10^{50}$  erg/s) for a WR (BSG). For instance, protons accelerated on the surface of either a WR or BSG may be expected under the condition that the jet would have a luminosity  $L_j \lesssim 10^{48}$  erg/s for both a WR and BSG. Otherwise, under the condition  $r_j < r_c$  protons cannot be expected inside the progenitors unless  $L > 10^{51}$  erg/s or/and  $t_\nu < 10^{-3}$  s and  $\Gamma > 40$  ( $\Gamma > 220$ ) for a WR (BSG). Comparing the acceleration and the synchrotron time scales, then the maximum energy achieved by accelerated protons in internal shocks with  $r_c < r_j$  and  $\tau \sim 1$  is given by eq. (9). Figure 4 shows neutrino energy (above 30 TeV) generated by p- $\gamma$  interactions at internal shocks inside of a WR (left;  $n_\gamma = 10^{16} \text{ cm}^{-3}$ ) and BSG (right;  $n_\gamma = 10^{13} \text{ cm}^{-3}$ ) for a luminosity in the range  $10^{46} \leq L \leq 10^{52}$  erg/s and four values of energy fraction going to accelerate electrons ( $\epsilon_e = 0.5, 5 \times 10^{-2}, 5 \times 10^{-3}$  and  $5 \times 10^{-4}$ ). Left panels exhibit that the maximum neutrino energy for  $L = 10^{52}$  erg/s and  $\epsilon_e = 0.5(5 \times 10^{-4})$  is  $E_\nu = 41.7(9.8) \times 10^{15}$  eV whereas the neutrino energy is  $E_\nu = 5.3(30.1) \times 10^{16}$  for  $L = 10^{46}$  erg/s and the same values considered of  $\epsilon_e$ . As shown in the right panels, the maximum neutrino energy is  $E_\nu = 1.4(8.1) \times 10^{14}$  eV for  $L = 10^{52}$  erg/s and  $\epsilon_e = 0.5(5 \times 10^{-4})$ , and  $E_\nu = 4.2(25.3) \times 10^{15}$  eV for  $L = 10^{46}$  erg/s. In panels can be observed a dashed line with  $E_\nu = 2.6$  PeV. This value of neutrino event can be obtained for  $L < 7.3 \times 10^{46}$  ( $7.1 \times 10^{49}$ ) erg/s and  $\epsilon_e < 0.5$  ( $5 \times 10^{-4}$ ) when considered a WR, whereas it is created for  $L < 10^{51}$  erg/s and  $\epsilon_e < 0.5$  in a BSG. Finally, based on the condition required for the proton ray acceleration (eq. 24), we have highlighted the region where parameters are restricted, as indicated in the plot labels.

Figure 5 shows neutrino energy (above 30 TeV) generated as charged kaon and pion decays in p-h interactions for  $10^{-4} \leq \epsilon_B \leq 10^{-1}$  (left) and  $10^{46} \leq L \leq 10^{52}$  erg/s (right). Left panel shows that the maximum neutrino energy is  $E_\nu < 3 \times 10^{13}$  ( $2.1 \times 10^{16}$ ) eV for  $\epsilon_B = 10^{-1}$  and  $E_\nu = 7.1 \times 10^{14}$  ( $> 10^{19}$ ) eV for  $\epsilon_B = 10^{-4}$ . Right panel exhibits that the maximum neutrino energy is  $E_\nu = 1.1 \times 10^{17}$  ( $4.5 \times 10^{21}$ ) eV for  $L = 10^{45}$  erg/s and  $E_\nu < 3 \times 10^{13}$  ( $5.8 \times 10^{14}$ ) eV for  $L = 10^{52}$  erg/s when neutrino is coming from pion (kaon) decay product inside WR (BSG). Putting a dashed line to mark the neutrino energy  $E_\nu = 2.6$  PeV, we can observe that for  $\epsilon_B < 10^{-3}$  ( $5.1 \times 10^{-3}$ ) neutrinos at this energy could be generated from decay product of pions (kaons) in a WR whereas for  $6.1 \times 10^{-3} \leq \epsilon_B \leq 0.1$  it could be created in a BSG. The right panel shows that depending on total luminosity, neutrinos coming from a WR and/or BSG could be created as pion and kaon decay products. In this panel, we show the region where parameters are restricted as showed in the plot label in accordance with the condition required for the proton acceleration (eq. 24).

Requiring the effective target mass of the IceCube experiment ([IceCube Collaboration 2013](#)), we use the method of Chi-square  $\chi^2$  minimization as implemented in the ROOT software package ([Brun & Rademakers 1997](#)) to fit the effective target mass as a function of neutrino energy. Then, the best function that describes the effective target mass is

$$M_{eff} = \begin{cases} f_6(E_\nu), & 1 \text{ TeV} < E_\nu < 950 \text{ TeV} \\ 5.19 \times 10^{-3} \left( \frac{E_\nu}{\text{TeV}} \right) + 3.86 \times 10^2, & 950 \text{ TeV} < E_\nu < 10^4 \text{ TeV}, \end{cases}$$



where

$$f_6(E_\nu) = 2.46 \times 10^{-15} \left( \frac{E_\nu}{\text{TeV}} \right)^6 - 1.99 \times 10^{-12} \left( \frac{E_\nu}{\text{TeV}} \right)^5 \\ - 1.09 \times 10^{-8} \left( \frac{E_\nu}{\text{TeV}} \right)^4 + 2.07 \times 10^{-5} \left( \frac{E_\nu}{\text{TeV}} \right)^3 \\ - 1.38 \times 10^{-2} \left( \frac{E_\nu}{\text{TeV}} \right)^2 + 3.91 \left( \frac{E_\nu}{\text{TeV}} \right) - 35.3.$$

It is worth noting that the muon neutrino of the effective target mass was used. Figure 6 shows the effective target mass of the IceCube experiment as a function of neutrino energy.

With the p- $\gamma$  spectrum (eq. 19) and using the method of Chi-square  $\chi^2$  minimization (Brun & Rademakers 1997), we have obtained the functions (eqs. A3, A4 and A5) that describe the parameters  $a_1$ ,  $a_2$  and  $a_3$ , respectively, as shown in Figure 7 and Appendix A.

Taking into account the target mass of the IceCube experiment (eq. 25), the p- $\gamma$  (eq. 19) and p-hadron (eq. 21) spectra, from eq. (18) we have computed the number of neutrinos expected in the IceCube detector. Figure 8 shows the number of neutrinos as a function of energy expected in the IceCube experiment from the p- $\gamma$  (above panels) and p-h (below panels) interactions for a source located at 10 Mpc. From p- $\gamma$  interactions we have used a target photon density  $n_\gamma \sim 10^{13} \text{cm}^{-3}$  whereas from p-h interactions a proton density target (as indicated in the label plots) was required. We compute the upper limit on the proton density in order to obtain one neutrino event at 2.6 PeV for typical values of the spectrum index of proton distribution ( $2.1 \leq \alpha \leq 2.3$ ).

## 5. CONCLUSIONS

In order to explain the multi-PeV neutrino, we have evoked p- $\gamma$  and p-h interaction model at internal shocks inside the IGRB progenitor stars. We have explored the set of parameter values:  $\Gamma$ ,  $t_\nu$ ,  $L$ ,  $\alpha$ ,  $\epsilon_B$  and  $\epsilon_e$  to explain the neutrino event at 2.6 PeV. We have computed the characteristic radius and the optical depth to which the shocked jet becomes cylindrical and the condition for proton acceleration inside the star is satisfied. We have found that protons can hardly be accelerated at internal shocks formed at the distance less than the cylindrical radius  $r_j < r_c$  unless  $L > 10^{51} \text{erg/s}$  or  $t_\nu < 10^{-3} \text{s}$  and  $\Gamma > 40$  ( $\Gamma > 220$ ) for a WR (BSG). Otherwise, protons at internal shocks under the condition  $r_c < r_j$  can be accelerated, thus interacting with hadrons and photons at this place. We have found that this neutrino could be created by p- $\gamma$  and p-h interactions with a total luminosity and internal shock radius in the range  $10^{46.5} \leq L \leq 10^{50.5} \text{erg/s}$  ( $10^{46} \leq L \leq 10^{49.8} \text{erg/s}$ ) and  $10^8 \leq r_j \leq 10^{11} \text{cm}$  ( $10^{10} \leq r_j \leq 10^{12.3} \text{cm}$ ), respectively, for a WR (BSG) with  $\Gamma \leq 40$  ( $\Gamma \leq 220$ ). Additionally, the values of equipartition parameters lie in the ranges  $\epsilon_e < 0.05$  and  $10^{-4} \leq \epsilon_B \leq 10^{-1}$  which could be a smaller range depending on the progenitor considered.

Recently, Murase & Ioka (2013) studied GeV - PeV neutrino production in collimated jets inside progenitors of GRBs, considering both collimation and internal shocks. They showed that although internal shocks in the collimated jet are less favorable for the cosmic ray acceleration than the collimation shocks, due to the meson radiative cooling HE neutrinos around 1 PeV can be only expected from internal shocks. Otherwise, HE neutrinos from the collimation shocks are expected around 10 TeV due to the strong meson cooling. They also found that unless  $\Gamma \gtrsim 10^3$ , cosmic rays and HE neutrinos are expected for high-power jets inside a WR. Authors showed that lIGRBs can be consistent with the astrophysical neutrino background reported by IceCube Collaboration. In this work, we have explored the values of total luminosity, internal shock radius, bulk Lorentz factor and the microphysical parameters so that CCSNe-GRB located at 10 Mpc (Ando & Beacom 2005) could create a 2.6-PeV neutrino event at internal shocks inside the star.

In hIGRBs copious target photons are expected for photo-hadronic interactions, making these GRBs promising candidates for neutrino detection. Searches for HE neutrinos in spatial and temporal coincidence around this population has been performed, although no neutrinos have been observed. The null neutrino result reported by IceCube Collaboration in some GRBs (Abbasi et al. 2012) could be explained based on the results obtained and showed in figs. (3), (4) and (5). We show that a multi-PeV neutrino event could be associated to IGRBs with  $L \sim 10^{50.5}$  ( $\sim 10^{50}$ ) erg/s provided that the internal shocks occur at  $\sim 10^9$  ( $\sim 10^{10.2}$ ) cm for a WR (BSG). Otherwise, this PeV neutrino is not expected from hIGRBs with  $\Gamma \ll 40$  ( $\Gamma \ll 220$ ) and/or internal shocks on the surface of WR (BSG).

By considering a range of GeV - TeV neutrino energies with a flux ratio of  $\dot{N}_{\nu_\mu} \simeq \dot{N}_{\bar{\nu}_\mu} \simeq 2\dot{N}_{\nu_e} \simeq 2\dot{N}_{\bar{\nu}_e}$ , Fraija (2015) studied the effect of thermal and magnetized plasma generated in internal shocks and the envelop of star on the neutrino oscillations. The author showed that the resonance lengths lie in the range  $l_{res} \sim (10^{12} \text{ to } 10^{14}) \text{cm}$ , hence depending on the progenitor associated (e.g. WR or SBG) and oscillation parameters, neutrinos would leave the internal shock region and the star in a different flavor to the original. Fraija (2015) found that although neutrinos from a few GeV to TeV can oscillate resonantly from one flavor to another, neutrino  $> \text{PeV}$  can hardly oscillate. Finally, he showed that a non-significant deviation of the standard flavor ratio (1:1:1) could be expected on Earth.

The number of sources with internal shocks inside the stars may be much larger than those exhibiting one. Within 10 Mpc, the rate of core-collapse supernovae is  $\sim 1 - 3 \text{yr}^{-1}$ , with a large contribution of galaxies around 3 - 4 Mpc. At larger distances, the expected number of neutrino events in the IceCube detector is still several, and the supernova rate could be  $\geq 10 \text{yr}^{-1}$  at 20 Mpc (Ando & Beacom 2005). Interference effects in the detector by atmospheric neutrino oscillation are very small (less than 10 %) due to the short path traveled by neutrinos in comparison with cosmological distances (Mena et al. 2007).

We thank C. Dermer, A. M. Sodelberg, B. Zhang, I. Taboada, K. Murase, W. H. Lee and F. de Colle for useful discussions,

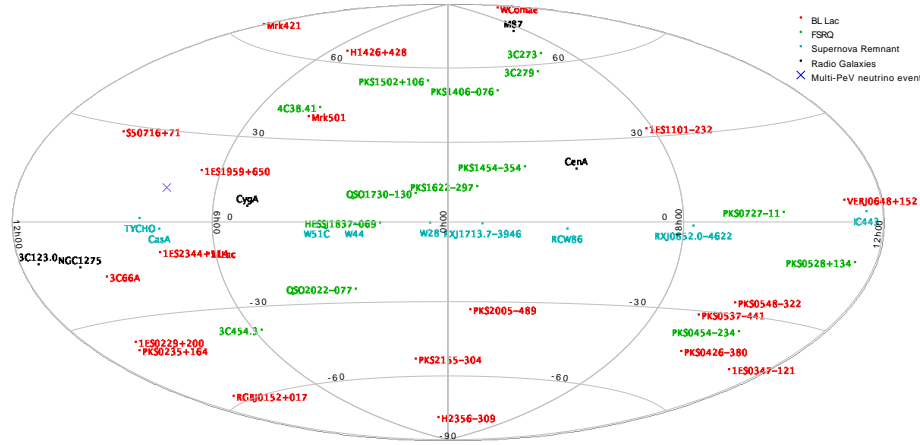


FIG. 1.— Sky-map with the location of BL Lac sources, FSRQs, Supernova Remnants, Radio Galaxies and the multi-PeV neutrino event detected by the IceCube detector (blue cross).

Anita Mücke and Antonio Galván for helping us to use the SOPHIA program and the TOPCAT team for the useful sky-map tools.

## REFERENCES

- Aartsen, M. G., Abbasi, R., Abdou, Y., et al. 2013, *Physical Review Letters*, 111, 021103
- Aartsen, M. G., Ackermann, M., Adams, J., et al. 2014, *Physical Review Letters*, 113, 101101
- Abbasi, R., Abdou, Y., Abu-Zayyad, T., et al. 2012, *Nature*, 484, 351
- Ando, S., & Beacom, J. F. 2005, *Physical Review Letters*, 95, 061103
- Böttcher, M., & Dermer, C. D. 1998, *ApJ*, 499, L131
- Bromberg, O., Mikolitzky, Z., & Levinson, A. 2011a, *ApJ*, 733, 85
- Bromberg, O., Nakar, E., & Piran, T. 2011b, *ApJ*, 739, L55
- Brun, R., & Rademakers, F. 1997, *Nuclear Instruments and Methods in Physics Research A*, 389, 81
- Budnik, R., Katz, B., Sagiv, A., & Waxman, E. 2010, *ApJ*, 725, 63
- Dermer, C. D., Murase, K., & Inoue, Y. 2014, *Journal of High Energy Astrophysics*, 3, 29
- Esmaili, A., & Dario Serpico, P. 2013, *J. Cosmology Astropart. Phys.*, 11, 54
- Feldstein, B., Kusenko, A., Matsumoto, S., & Yanagida, T. T. 2013, *Phys. Rev. D*, 88, 015004
- Frajia, N. 2014, *MNRAS*, 437, 2187
- . 2015, *MNRAS*, 450, 2784
- Gandhi, R., Quigg, C., Reno, M. H., & Sarcevic, I. 1998, *Phys. Rev. D*, 58, 093009
- Gendre, B., Stratta, G., Atteia, J. L., et al. 2013, *The Astrophysical Journal*, 766, 30
- Huang, Y. F., Dai, Z. G., & Lu, T. 2002, *MNRAS*, 332, 735
- IceCube Collaboration. 2013, *Science*, 342, 0
- Ioka, K., & Murase, K. 2014, *Progress of Theoretical and Experimental Physics*, 2014, 060001
- Katz, B., Budnik, R., & Waxman, E. 2010, *ApJ*, 716, 781
- Kelner, S. R., & Aharonian, F. A. 2008, *Phys. Rev. D*, 78, 034013
- Kelner, S. R., Aharonian, F. A., & Bugayov, V. V. 2006, *Phys. Rev. D*, 74, 034018
- Levinson, A. 2012, *ApJ*, 756, 174
- Liang, E., Zhang, B., Virgili, F., & Dai, Z. G. 2007, *The Astrophysical Journal*, 662, 1111
- Liu, R.-Y., & Wang, X.-Y. 2013, *ApJ*, 766, 73
- MacLachlan, G. A., Shenoy, A., Sonbas, E., et al. 2013, *MNRAS*, 432, 857
- Mena, O., Mocioiu, I., & Razzaque, S. 2007, *Phys. Rev. D*, 75, 063003
- Mészáros, P. 2006, *Reports on Progress in Physics*, 69, 2259
- Mészáros, P., & Waxman, E. 2001, *Phys. Rev. Lett.*, 87, 171102
- Milgrom, M., & Usov, V. 1995, *ApJ*, 449, L37
- Mizuta, A., & Ioka, K. 2013, *ApJ*, 777, 162
- Murase, K. 2008, *Phys. Rev. D*, 78, 101302
- Murase, K., & Ioka, K. 2013, *Physical Review Letters*, 111, 121102
- Murase, K., Ioka, K., Nagataki, S., & Nakamura, T. 2006, *ApJ*, 651, L5
- Ng, K. C. Y., & Beacom, J. F. 2014, *Phys. Rev. D*, 90, 065035
- Padovani, P., Petropoulou, M., Giommi, P., & Resconi, E. 2015, *MNRAS*, 452, 1877
- Petropoulou, M., Dimitrakoudis, S., Padovani, P., Mastichiadis, A., & Resconi, E. 2015, *MNRAS*, 448, 2412
- Petropoulou, M., Giannios, D., & Dimitrakoudis, S. 2014, *MNRAS*, 445, 570
- Rachen, J. P., & Mészáros, P. 1998, *Phys. Rev. D*, 58, 123005
- Razzaque, S. 2013, *Phys. Rev. D*, 88, 103003
- Razzaque, S., Mészáros, P., & Waxman, E. 2005, *Modern Physics Letters A*, 20, 2351
- Razzaque, S., & Smirnov, A. Y. 2010, *Journal of High Energy Physics*, 3, 31
- Rees, M. J., & Mészáros, P. 2005, *ApJ*, 628, 847
- Schoenen, S., & Raedel, L. 2015, *The Astronomer's Telegram*, 7856, 1
- Soderberg, & et al. 2006, *Nature*, 442, 1014
- Soderberg, A. M., & et al. 2010, *Nature*, 463, 513
- Stecker, F. W. 2013, *Phys. Rev. D*, 88, 047301
- Tamborra, I., & Ando, S. 2015a, *J. Cosmology Astropart. Phys.*, 9, 36
- . 2015b, *ArXiv e-prints*, arXiv:1512.01559
- Vietri, M. 1997, *Physical Review Letters*, 78, 4328
- Waxman, E. 1995a, *Physical Review Letters*, 75, 386
- . 1995b, *ApJ*, 452, L1
- . 2000a, *ApJS*, 127, 519
- . 2000b, *Nuclear Physics B Proceedings Supplements*, 87, 345
- Waxman, E., & Bahcall, J. 1999, *Phys. Rev. D*, 59, 023002
- Zhang, B., & Mészáros, P. 2004, *International Journal of Modern Physics A*, 19, 2385

## APPENDIX

### A. FUNCTION $F_{\nu\mu}^{P\gamma}$

The function  $F^{P\gamma}(\eta, x)$  given in eq. (19) is (Kelner & Aharonian 2008)

$$F_{\nu\mu}^{P\gamma}(\eta, x) = a_1 \exp \left\{ -a_2 \left[ \log \left( \frac{x}{x_1} \right) \right]^{a_3} \right\} \left[ \log \left( \frac{2}{1+y^2} \right) \right]^\psi, \quad (\text{A1})$$

where  $\psi = 2.5 + 1.4 \log \left( \frac{\eta}{\eta_0} \right)$  with  $\eta = \frac{4\epsilon E_p}{m_p^2}$  and  $\eta_0 = 2 \frac{m_\pi}{m_p} + \frac{m_\pi^2}{m_p^2} \simeq 0.313$ . The variables  $y$  and  $x$  are

$$y = \frac{x - x_1}{x_2 - x_1} \quad \text{and} \quad x = \frac{E_\nu}{E_p}, \quad (\text{A2})$$

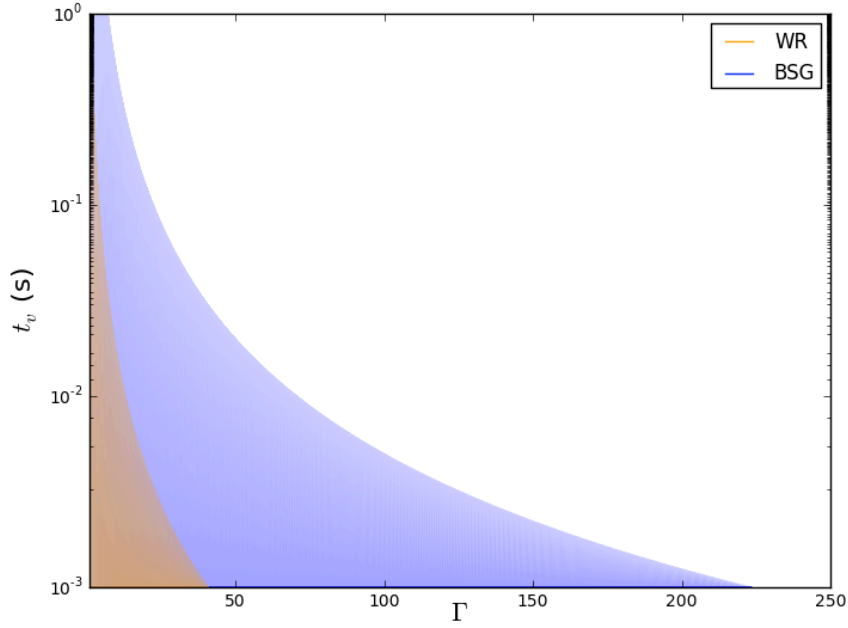


FIG. 2.— Set of values of variability and bulk Lorentz factor for which internal shocks take places inside a WR (red region) and BSG (blue region).

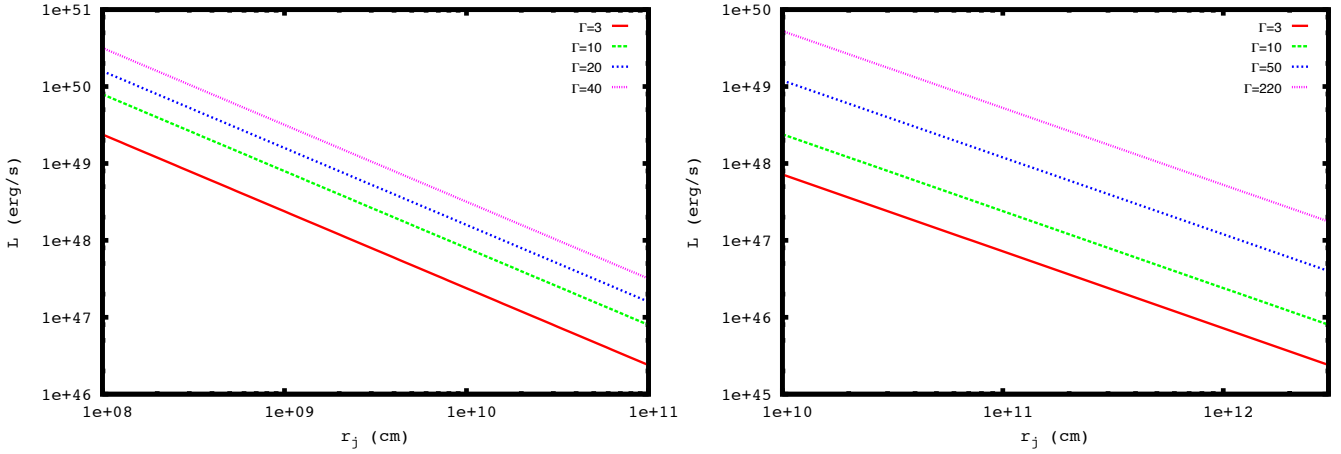


FIG. 3.— Necessary condition for proton acceleration (eq. 8) when we consider a WR (left) and BSG (right).

respectively. The appropriate parameters of the distribution for muon neutrino are:  $x_1 = 0.427 x_-$  and

$$x_2 = \begin{cases} 0.427 x_+ , & \eta/\eta_0 < 2.14 \\ [0.427 + 0.00729(\eta/\eta_0 - 2.14)] x_+ , & 2.14 < \eta/\eta_0 < 10 \\ x_+ , & \eta/\eta_0 > 10. \end{cases}$$

The values of  $x_{\pm}$  correspond to the maximum and minimum pion energies,  $x_{\pm} = \frac{1}{2(1+\eta)} [\eta + r^2 \pm \sqrt{(\eta - r^2 - 2r)(\eta - r^2 + 2r)}]$  with  $r = m_{\pi}/m_p \approx 0.146$ .

In accordance with the values  $a_1$ ,  $a_2$  and  $a_3$  given in Kelner & Aharonian (2008) and using the method of Chi-square  $\chi^2$  minimization (Brun & Rademakers 1997), the best fit of the numerical values of parameters  $a_1$ ,  $a_2$  and  $a_3$  are

$$a_1 = 1.63 \times 10^{-18} \left( \frac{\eta}{\eta_0} \right)^2 + 1.49 \times 10^{-16} \left( \frac{\eta}{\eta_0} \right) - 1.65 \times 10^{-16} , \quad (A3)$$

$$a_2 = \begin{cases} f_6 \left( \frac{\eta}{\eta_0} \right) , & 1 < \eta/\eta_0 < 9 \\ 1.94 \times 10^{-5} \left( \frac{\eta}{\eta_0} \right)^2 - 2.87 \times 10^{-3} \left( \frac{\eta}{\eta_0} \right) + 0.14 & \eta/\eta_0 > 9. \end{cases}$$



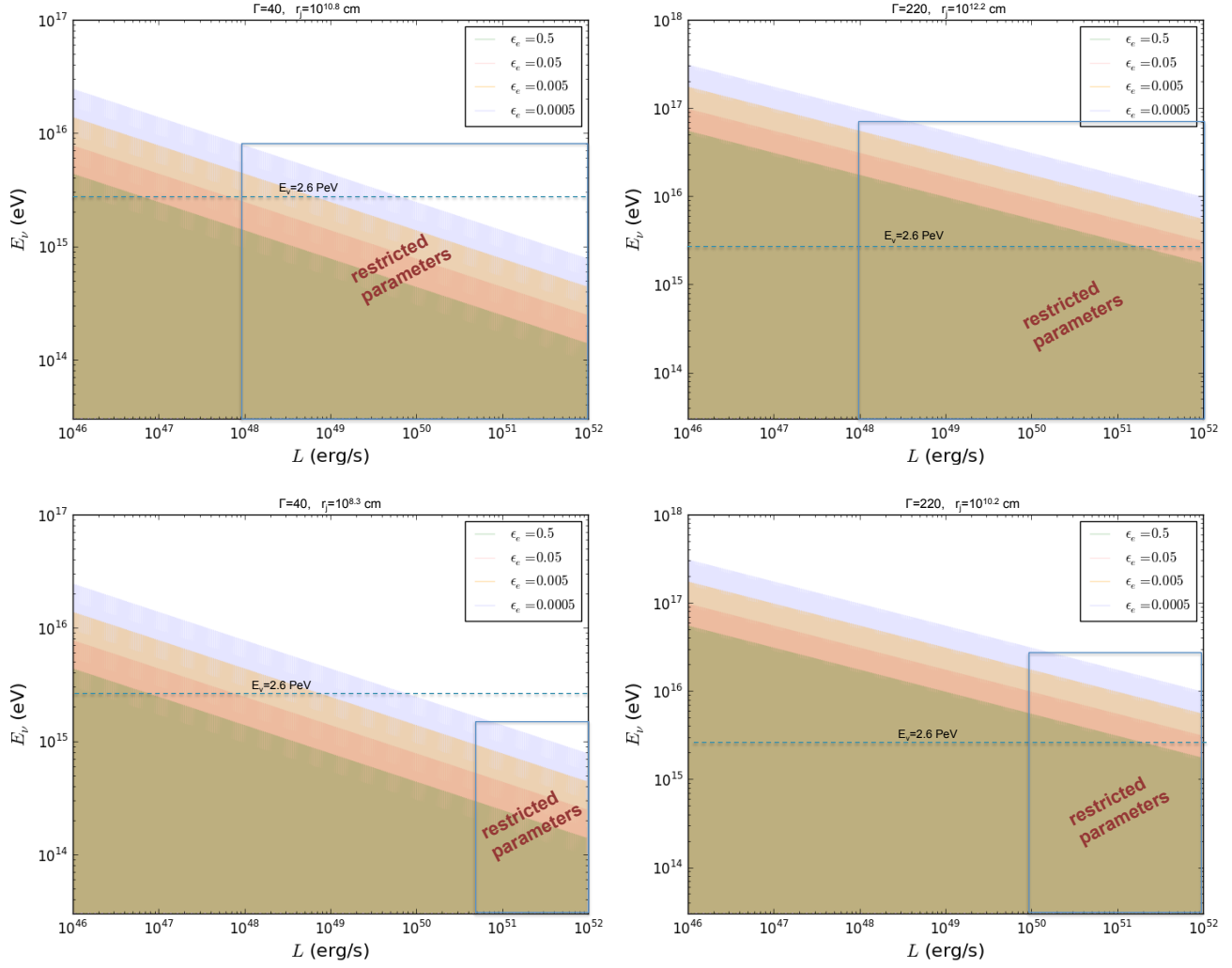


FIG. 4.— Neutrino energy as a function of luminosity generated by p- $\gamma$  interactions at internal shocks inside of a WR (left) and BSGs (right).

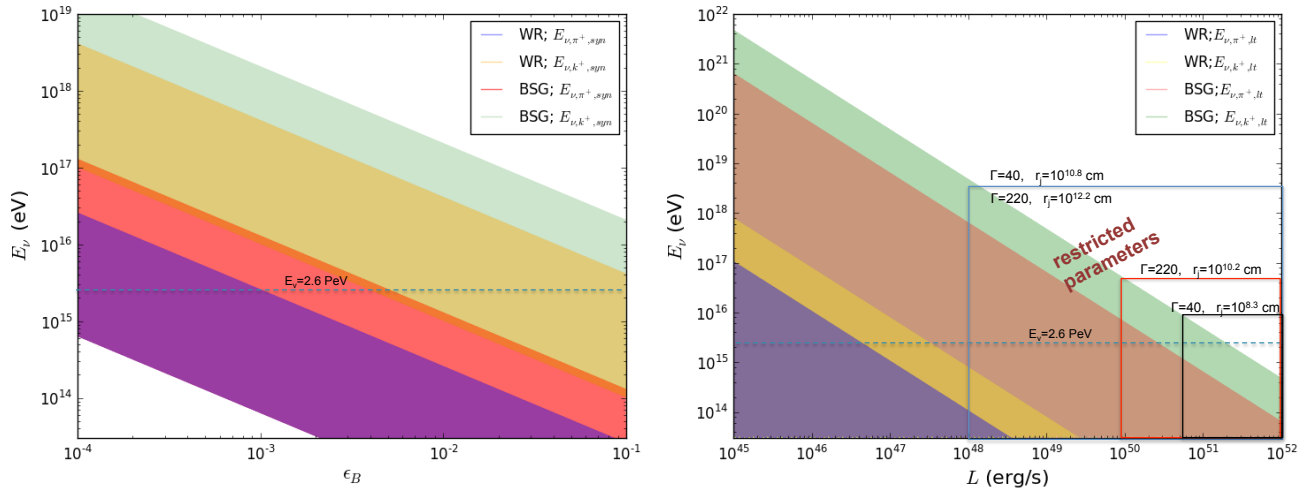


FIG. 5.— Neutrino energy generated by p-h interactions at internal shocks. synchrotron (left) and lifetime (right).

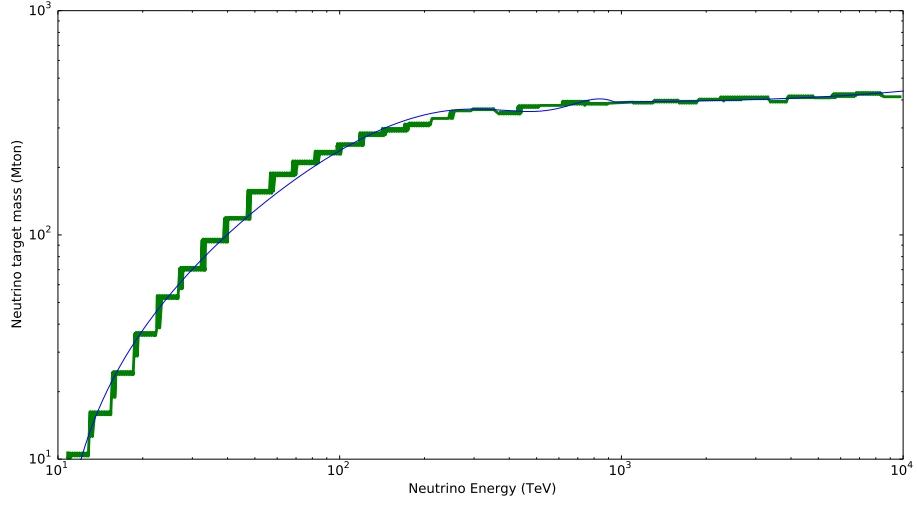


FIG. 6.— Effective target mass of the IceCube experiment as a function of neutrino energy (green line; [IceCube Collaboration \(2013\)](#)). Line in blue color represents the function used to fit the effective target mass.

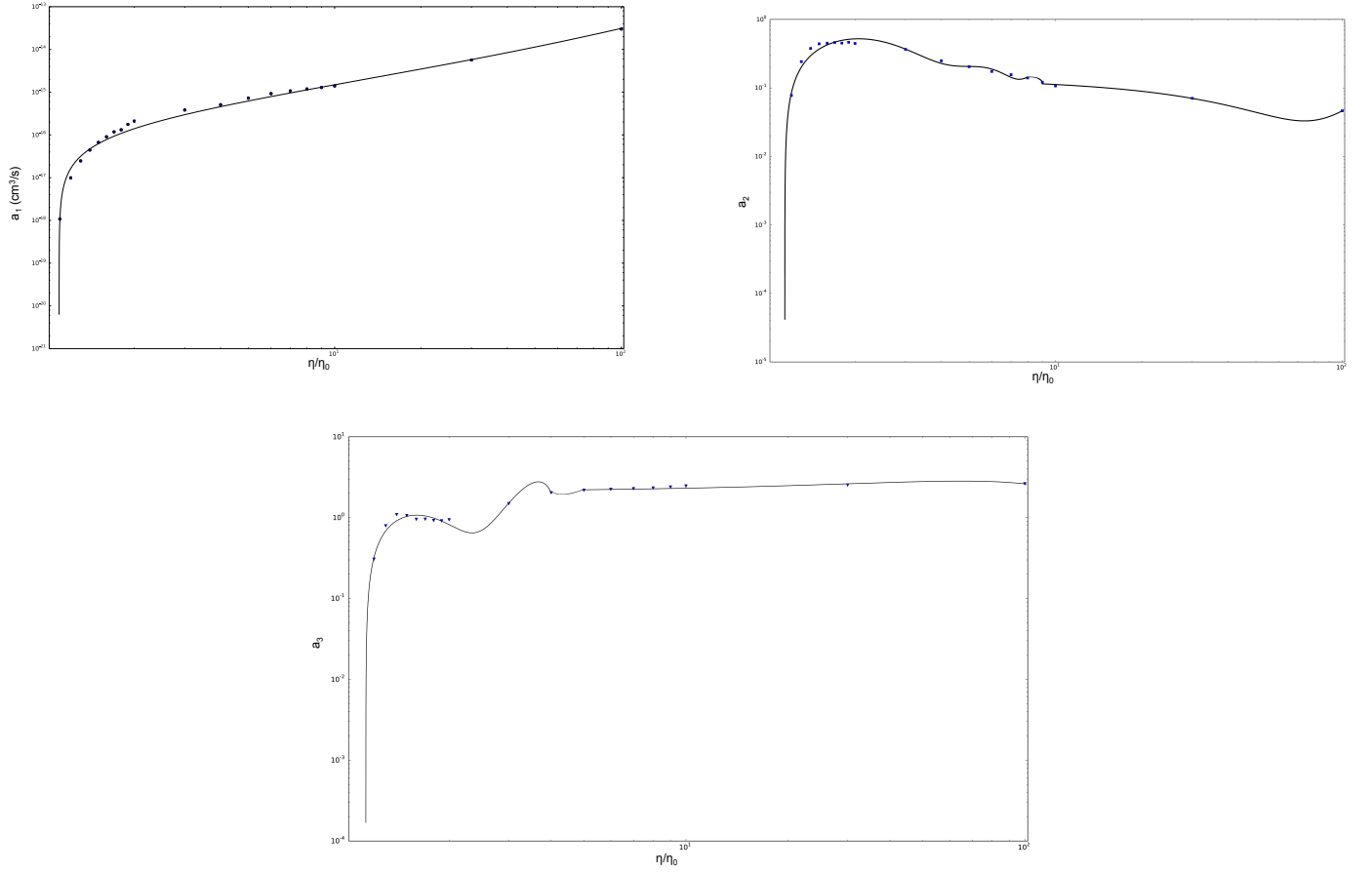


FIG. 7.— Fit of numerical values of parameters  $a_1$ ,  $a_2$  and  $a_3$  characterizing the neutrino spectrum ([Kelner & Aharonian 2008](#)).

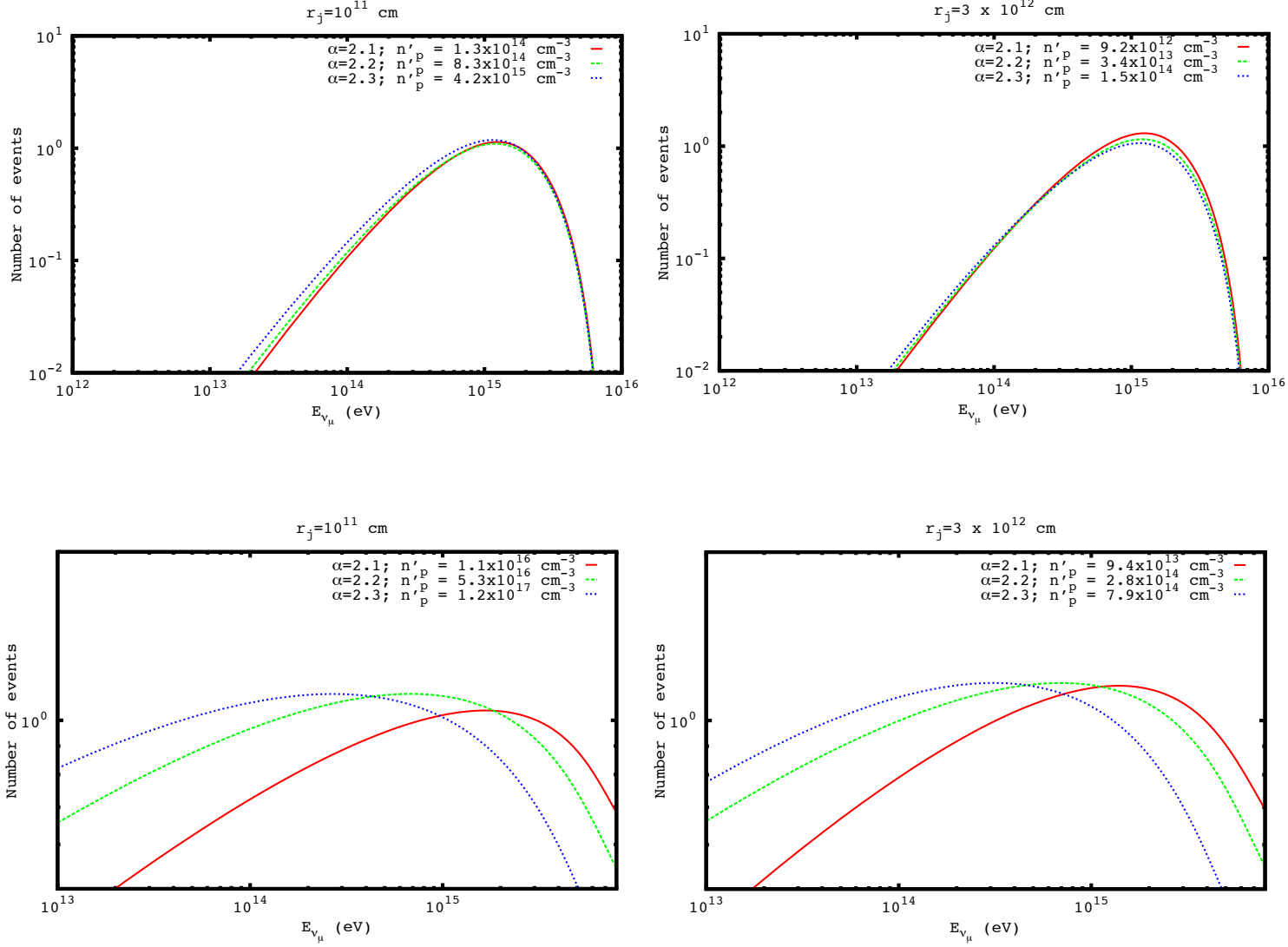


FIG. 8.— Number of events as a function of neutrino energy expected in the IceCube experiment from the p- $\gamma$  (above panels) and p-h (below panels) interactions.

with

$$f_6\left(\frac{\eta}{\eta_0}\right) = -3.88 \times 10^{-4} \left(\frac{\eta}{\eta_0}\right)^6 + 1.30 \times 10^{-2} \left(\frac{\eta}{\eta_0}\right)^5 - 0.17 \left(\frac{\eta}{\eta_0}\right)^4 + 1.19 \left(\frac{\eta}{\eta_0}\right)^3 - 4.26 \left(\frac{\eta}{\eta_0}\right)^2 + 7.47 \left(\frac{\eta}{\eta_0}\right) - 4.46 \quad (\text{A4})$$

and

$$a_3 = \begin{cases} f_4\left(\frac{\eta}{\eta_0}\right), & 1 < \eta/\eta_0 < 4 \\ -1.74 \times 10^{-4} \left(\frac{\eta}{\eta_0}\right)^2 + 2.25 \times 10^{-2} \left(\frac{\eta}{\eta_0}\right) + 2.10 & \eta/\eta_0 > 4. \end{cases}$$

with

$$f_4\left(\frac{\eta}{\eta_0}\right) = -0.97 \left(\frac{\eta}{\eta_0}\right)^4 + 9.81 \left(\frac{\eta}{\eta_0}\right)^3 - 3.52 \times 10 \left(\frac{\eta}{\eta_0}\right)^2 + 53.32 \left(\frac{\eta}{\eta_0}\right) - 27.81 \quad (\text{A5})$$

respectively.

B. FUNCTION  $F_{\nu_\mu}^{PP}$ 

The function  $F_{\nu_\mu}^{PP}$  is split in two parts (Kelner et al. 2006): one coming from the pion decay  $\pi \rightarrow \mu \nu_\mu$  ( $F_{\nu_\mu^{(1)}}^{PP}$ ) and the other comes from decay of muon  $\mu \rightarrow e \bar{\nu}_e \nu_\mu$  ( $F_{\nu_\mu^{(2)}}^{PP}$ ).

B1.  $F_{\nu_\mu^{(1)}}^{PP}$  from pion decay

The spectrum of muonic neutrino generated through de direct decay of pion can be written as

$$F_{\nu_\mu^{(1)}} = b_1 \frac{\log z}{z} \left( \frac{1 - z^{b_2}}{1 + b_3 z^{b_2} (1 - z^{b_2})} \right)^4 \times \left[ \frac{1}{\log z} - \frac{4b_2 z^{b_2}}{1 - z^{b_2}} - \frac{4b_3 b_2 z^{b_2} (1 - 2z^{b_2})}{1 + b_3 z^{b_2} (1 - z^{b_2})} \right], \quad (\text{B1})$$

where the variables  $z$  and  $x$  are  $z = \frac{x}{0.427}$  and  $x = \frac{E_\nu}{E_p}$ , respectively. The parameters  $b_1$ ,  $b_2$  and  $b_3$  are

$$b_1 = 1.75 + 0.204 S + 0.010 S^2, \quad (\text{B2})$$

$$b_2 = \frac{1}{1.67 + 0.111 S + 0.0038 S^2}, \quad (\text{B3})$$

and

$$b_3 = 1.07 - 0.086 S + 0.002 S^2, \quad (\text{B4})$$

with  $S = \log(E_p/TeV)$ .

B2.  $F_{\nu_\mu^{(2)}}^{PP}$  from muon decay

The spectrum of muonic neutrino generated through de direct decay of muon can be written as

$$F_{\nu_\mu^{(2)}} = c_1 \frac{[1 + c_3 (\log x)^2]^3}{x (1 + \frac{0.3}{x^{c_2}})} (-\log x)^5 \quad (\text{B5})$$

where the parameters  $c_1$ ,  $c_2$  and  $c_3$  are

$$c_1 = \frac{1}{69.5 + 2.65 S + 0.3 S^2}, \quad (\text{B6})$$

$$c_2 = \frac{1}{(0.201 + 0.0062 S + 0.00042 S^2)^{1/4}}, \quad (\text{B7})$$

and

$$c_3 = \frac{0.279 + 0.141 S + 0.0172 S^2}{0.3 + (2.3 + S)^2}. \quad (\text{B8})$$